

Improved Accuracy for 3D Ego-Motion Estimation Using Automotive FMCW MIMO Radar

Yuan, Sen; Wang, Dingyang; Fioranelli, Francesco; Yarovoy, Alexander

DOI

[10.1109/RadarConf2458775.2024.10548030](https://doi.org/10.1109/RadarConf2458775.2024.10548030)

Publication date

2024

Document Version

Final published version

Published in

Proceedings of the 2024 IEEE Radar Conference (RadarConf24)

Citation (APA)

Yuan, S., Wang, D., Fioranelli, F., & Yarovoy, A. (2024). Improved Accuracy for 3D Ego-Motion Estimation Using Automotive FMCW MIMO Radar. In *Proceedings of the 2024 IEEE Radar Conference (RadarConf24)* (Proceedings of the IEEE Radar Conference). IEEE.
<https://doi.org/10.1109/RadarConf2458775.2024.10548030>

Important note

To cite this publication, please use the final published version (if applicable).
Please check the document version above.

Copyright

Other than for strictly personal use, it is not permitted to download, forward or distribute the text or part of it, without the consent of the author(s) and/or copyright holder(s), unless the work is under an open content license such as Creative Commons.

Takedown policy

Please contact us and provide details if you believe this document breaches copyrights.
We will remove access to the work immediately and investigate your claim.

Green Open Access added to TU Delft Institutional Repository

'You share, we take care!' - Taverne project

<https://www.openaccess.nl/en/you-share-we-take-care>

Otherwise as indicated in the copyright section: the publisher is the copyright holder of this work and the author uses the Dutch legislation to make this work public.

Improved Accuracy for 3D Ego-motion Estimation using Automotive FMCW MIMO radar

Sen Yuan, Dingyang Wang, Francesco Fioranelli and Alexander Yarovoy

*Department of Microelectronics, Microwave Sensing Signals & Systems (MS3) Group
Delft University of Technology (TU Delft), Delft, The Netherlands
{S.Yuan-3, D.Wang-6, F.Fioranelli, A.Yarovoy}@tudelft.nl*

Abstract—The problem of 3D ego-motion velocity estimation using multichannel Frequency Modulated Continuous Wave (FMCW) radar sensors has been studied. Special attention is given to presence of moving targets in the scene. These targets are first distinguished by the difference between the measured Doppler, and the Doppler calculated with an initial rough estimation of the vehicle ego-velocity. Then, an iterative algorithm is proposed to reduce the influence of the moving targets in the ego-motion estimation procedure, thus improving the overall accuracy. The performance of the proposed algorithm is compared with state-of-the-art alternatives based on simulated data, and superior performance has been demonstrated.

Index Terms—Ego-motion estimation, multi-channel radar, velocity measurement, automotive radar.

I. INTRODUCTION

Ego-motion estimation is very essential for automotive industry and robotics. Many approaches to this problem have emerged, leveraging a variety of sensors such as vision, laser, Global Positioning System (GPS), Inertial Measurement Unit (IMU) sensors and wheel-based odometry. However, among those sensors, radar can offer precise and direct measurements of range, relative velocity, and angle for multiple targets, even in challenging weather and lighting conditions [1]. As a result, radar sensors receive significant attention and interest for localization and ego-motion estimation applications.

When addressing the problem of ego-motion estimation, a current trend in automotive is information fusion from different sensors, such as radar with Inertial Measurement Unit (IMU) [2]–[5], or with monocular Visual Inertial Odometry or monocular Thermal Inertial Odometry [6], and digital map databases [7]. Other methods focus on improving the estimation performance given by the radar sensor itself. These methods can be mainly categorized into model-based [8]–[10], normal distribution transform (NDT) [11], and Simultaneous Localization and Mapping (SLAM) approaches [12]–[15]. All these approaches require radar point clouds, which are generated after several data processing steps. At least one coherent processing interval, i.e. one frame, is required to create point clouds, which limits the possible update rate. Also, the data association between different frames is probabilistic based, which may introduce errors during the process.

Our previous work [12] proposed a method for ego-motion estimation starting from the lower signal level (i.e., the radar base-band signal before range-Doppler processing)

and achieved the best performance among the compared approaches. Using algorithms implemented directly at the signal level for ego-motion estimation, it can be easier to combine them with other high-resolution imaging algorithms [16] or automotive synthetic-aperture radar (SAR) algorithms [17], [18] to improve the performances for other tasks. However, the performance of the proposed algorithm relies highly on the assumption of static scene. By increasing the ratio of moving targets in the scene, the algorithm performance will decrease. Addressing this limitation is the major focus of this paper. Here, an iterative algorithm is proposed to reduce the influence of moving targets in the scene at the ego-motion estimation, thus improving its accuracy. Initially, a rough ego-motion estimation is performed. Then, the ego-motion induced Doppler for each target is iteratively compared with the measured Doppler. By doing so, the moving targets will be distinguished and discarded for later processing. A significant improvement is obtained in terms of ego-motion estimation accuracy, as demonstrated on multiple simulated tests.

The rest of the paper is organized as follows. In Section II, the signal model for a moving radar with 3 degrees of freedom is provided. The fundamentals of how to estimate the ego-motion velocity via the proposed optimization approach are explained in Section III. The simulation results for targets under different settings are provided in Section IV. Finally, conclusions are drawn in Section V.

II. FUNDAMENTAL CONCEPTS

A. Signal model

The proposed algorithm works for any multi-channel Frequency Modulated Continuous Wave (FMCW) radars, which has no requirements for the layout of antenna array. For automotive applications, we consider a FMCW multiple-input and multiple-output (MIMO) radar with N_a and N_e virtual array elements for azimuth and elevation estimation, respectively. Without losing generality, the omnidirectional antenna pattern is considered for the transmitter and receiver. The 2-D MIMO array is placed in the Y-Z plane, with the X-axis pointing towards the illuminated scene, as shown in Fig. 1.

The received radar signal is the sum of the reflected signals by the scatter points in the field of view. After reception, the signal will be mixed with the transmitted signal to obtain the

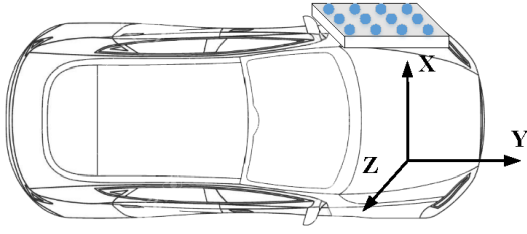


Fig. 1. The geometry of the side-looking automotive radar, where Y is the forward direction, X is the cross-forward direction, and Z is the elevation direction, satisfying the left-handed Cartesian coordinates.

baseband signal (dechirping). The dechirped discretized signal of the radar will be:

$$z(i, j, l, b) = \sum_o^k \alpha_o \exp[j\Phi(o, i, j)] \times \exp[-j2\pi(f_{d,o}Tl + \mu \frac{\gamma_o b}{f_s})] \quad (1)$$

where z is the radar received signal; o is the target's index; i and j are the index of the antenna elements counted from the 1st antenna element in azimuth and elevation direction, respectively; $l = 0, 1, 2, \dots, L_d - 1$ is the slow time index; L_d is the total number of the chirps in one frame; $b = 0, 1, 2, \dots, B_d - 1$ and $B_d = T_c f_s$ is the maximum number of samples within one chirp; f_s is the sampling frequency; T_c is the chirp duration; α_o is the constant complex amplitude related to the characteristics of the target o ; d is the space interval between adjacent antenna elements; c is the speed of light; θ_o is the azimuth of target o ; v_o is the radial velocity between target o and radar; μ is the frequency modulation rate; $\gamma_o = \frac{2D_o}{c} \ll T_c$ with D_o being the distance between antenna and target o ; $f_{d,o} = f_0 \frac{2v_o}{c}$ is the Doppler of the target o ; f_0 denotes the starting frequency of the chirp. The term Φ is the phase difference between different antenna pairs, which is related to the position of the radar mounted.

$$\Phi(o, i, j) \approx 2\pi f_0 (\frac{id}{c} \sin\theta_o \cos\phi_o + \frac{jd}{c} \sin\phi_o) \quad (2)$$

where $d = \frac{\lambda}{2}$, λ is the wavelength, and θ_o and ϕ_o are the target's azimuth and elevation angle.

B. Ego-motion estimation

Current ego-motion estimation algorithms rely on the spatial alignment between different processing time intervals. Many algorithms, e.g., NDT [11] or Matrix Inversion [9], were proposed, but still suffered from errors in the data alignment. It is reasonable to assume that in a short time, i.e., in one coherent processing interval or frame, a target will be in the same position at the range-Doppler diagram, (in other words, no target migration is assumed). The whole frame duration is then divided into two sub-intervals, starting from time u_0 and u_1 , where two subsequent range-Doppler indices can be

obtained from the detections. The ego-motion estimation can be performed via the data alignment by equating the two detected indices. The complete explanation of this approach is reported in [12], with the main components summarized here.

As mentioned, a 2D constant false alarm rate (CFAR) detection is performed on the range-Doppler spectrum, 2D FFT of the signal z in (1), which is expressed by:

$$Z(i, j, m, n, u) = \sum_o^k \alpha_o \pi^2 T_c f_s N_L \text{sinc}(\frac{(mT_c f_s + \mu \gamma_o T_c)}{2}) \times \text{sinc}(\frac{(n + f_{d,o}T)N_L}{2}) \times \exp[j\Phi(o, i, j, l)] \times \exp[-j\pi((mT_c f_s + \mu \gamma_o T_c) + (n + f_{d,o}T)(2u + N_L))] \quad (3)$$

where m and n are the indices of the frequency in range and Doppler domain, respectively; u is the starting index of the sub-intervals. Because of the *sinc* function in the expression, the amplitude peak will change according to the Doppler velocity and range of targets, which is at the basis of the subsequent detection processing.

Assuming that each range-Doppler cell only contains one target, which is reasonable because of the high resolution in the Doppler domain, the signal of the detected target at indices $[m_k, n_k]$ can be written as:

$$Z(i, j, m_k, n_k, u) \propto Z(1, 1, m_k, n_k, u) \exp[j\Phi(o_k, i, j, u)] \quad (4)$$

$$\Phi(o_k, i, j, u) = 2\pi f_0 (\frac{id}{c} \sin\hat{\theta}_{o_k}(u) \cos\hat{\phi}_{o_k}(u) + \frac{jd}{c} \sin\hat{\phi}_{o_k}(u)) \quad (5)$$

where m_k and n_k indicates the detected targets' range and Doppler index. Based on this equation, the spatial angles $\hat{\theta}_{o_k}(u)$ and $\hat{\phi}_{o_k}(u)$ of the detected targets can be obtained via pattern search [19].

After obtaining an estimation of the detected targets' elevation and azimuth for the sub-interval starting from time index u_0 , the indices for the targets will be the same as for the following sub-interval starting from time index u_1 . Thus, the detected targets for these intervals u_0 and u_1 are related as:

$$Z(i, j, m_k, n_k, u_1) \propto Z(i, j, m_k, n_k, u_0) \exp[j\Gamma(o_k, u_1, u_0)] \quad (6)$$

$$\Gamma(o_k, u_1, u_0) = 4\pi \frac{dr_{o_k} f_0}{c} \quad (7)$$

where $dr_{o_k} = V_d * (u_1 - u_0) = \hat{v}_{rx} * (u_1 - u_0) \cos\hat{\theta}_{o_k}(u) \cos\hat{\phi}_{o_k}(u) + \hat{v}_{ry} * (u_1 - u_0) \sin\hat{\theta}_{o_k}(u) \cos\hat{\phi}_{o_k}(u) + \hat{v}_{rz} * (u_1 - u_0) \sin\hat{\phi}_{o_k}(u)$. Essentially, the signal phase differences in the two sub-intervals are due to a displacement term in Γ , which is related to the relative ego speed $\hat{v}_{rx}, \hat{v}_{ry}, \hat{v}_{rz}$ between the radar and the targets, specifically the ego-motion velocity components

when all targets are static, which can be estimated by pattern search [19] as well.

A limitation of this method is the detrimental effect that detected moving targets will have on the ego-motion estimation. This issue is addressed in the next section.

III. PROBLEM FORMULATION AND PROPOSED METHOD

A. Problem formulation

Moving targets in the scene will introduce additional Doppler components, so that the velocity V_d in our signal model (7) will be the combination of the vehicle ego-motion and the targets' motion. Most of the Doppler-based algorithms in automotive, such as Doppler beam sharpening, SLAM and SAR implementations, will be affected by this. Also the ego-motion estimation presented in the previous section [12] will be affected, and the model for dr_{o_k} in equation (7) will face the mismatch problem and degrade the estimation results. Given the diversity of moving target classes and their motion models in automotive, it will be challenging to reduce their effect in the ego-motion estimation process.

B. Proposed method

To reduce the moving targets' influence, a feedback loop is added to the flow chart of the proposed iterative method, as shown in Fig. 3. The Doppler/velocity estimation $V_{dd}(m_k, n_k)$ will be obtained from the range-Doppler spectrum detections. The iteration will be at first initialized with the first rough estimation from (6), i.e., the Doppler/velocity estimation $V_{dd}(m_k, n_k)$. During each iteration, all the detected targets will be iteratively divided into virtual static targets group and virtual moving targets group. Only the static targets will be processed to derive more accurate ego-velocity estimation results. Specifically, the proposed method contains two important steps: first is the updating of the static targets' group; second is the breaking point to end the iterations.

1) *Updating of the static targets' group:* The vector $[v_x^i, v_y^i, v_z^i]$ is the velocity estimation from the i -th iteration. Knowing each target's position $[\theta_k, \phi_k]$, the target's ego-motion induced Doppler/velocity can be calculated as:

$$V_{ed}^{i+1}(m_k, n_k) = v_x^i \cos \theta_k \cos \phi_k + v_y^i \sin \theta_k \cos \phi_k + v_z^i \sin \phi_k \quad (8)$$

An example of the motion-induced velocity results and the detected velocity are drawn in Fig. 2, where differences between these two values due to the movement of targets are visible. The velocity difference $D_V^i(m_k, n_k) = V_{ed}^i(m_k, n_k) - V_{dd}(m_k, n_k)$ is defined as the difference between the ego-motion induced velocity V_{ed} and the velocity obtained from the spectrum V_{dd} . If the difference between the ego-motion induced velocity and the velocity obtained from the spectrum is higher than a certain threshold, the target will be marked as moving target. This label is obtained from the last iteration and shown as follows:

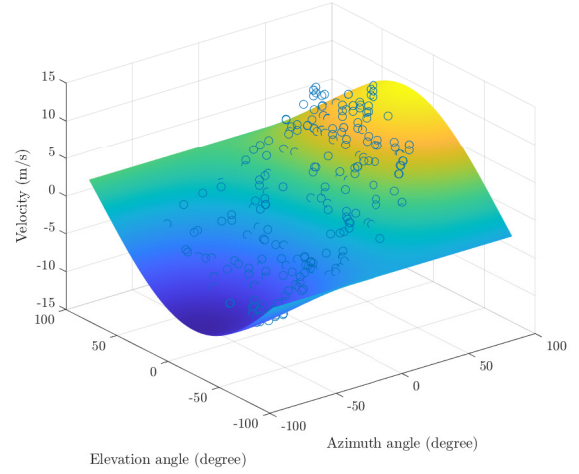


Fig. 2. An example of estimated velocity surface plot with the detections and calculated motion-induced velocity values. The blue points denote the detection results, while the surface plot shows the motion-induced velocity value in each azimuth-estimation position.

$$Label(m_k, n_k) = \begin{cases} static & |D_V^{i+1}(m_k, n_k)| \leq D_c E(|D_V^i|) \\ moving & |D_V^{i+1}(m_k, n_k)| > D_c E(|D_V^i|) \end{cases} \quad (9)$$

The static targets will be stacked together to form the matrix for translational motion $\mathbf{T}_t^{i+1}(u) \in \mathbb{C}^{N_a * N_e \times N_k}$ according to [12], and an optimization algorithm will be implemented to derive the new estimation $[v_x^{i+1}, v_y^{i+1}, v_z^{i+1}]$.

2) *Breaking point to end the iteration:* To ensure the number of iterations is enough to provide accurate estimation, different criteria are proposed here to define the threshold, namely Averaging-based-threshold (ABT), Ordered Statistics threshold (OST), and Ordered Statistics Averaging based threshold (OS-ABT),

Averaging based threshold (ABT):

$$E(abs(D_V^{i+1}(m_k, n_k))) - E(abs(D_V^i(m_k, n_k))) < \epsilon \quad (10)$$

where ϵ is the tolerant distance of moving targets, E is the operation of expectation.

Ordered Statistics threshold (OST): The velocity differences D_V^* will be sorted according to their amplitude. A new sequence of the variables is defined as:

$$D_V^*(1) \leq D_V^*(2) \leq \dots \leq D_V^*(K) \quad (11)$$

The iterations will then stop when:

$$D_V^{i+1}(k_{os}) - D_V^i(k_{os}) < \epsilon \quad (12)$$

Ordered Statistics Averaging based threshold (OS-ABT): The velocity differences D_V^* will be sorted as well to get the new sequence. To avoid some extreme case errors, the average is calculated after sorting. The iterations will then stop when:

$$E(D_V^{i+1}(1 : k_{os})) - E(D_V^i(1 : k_{os})) < \epsilon \quad (13)$$

where $(1 : k_{os})$ denotes the values from the first to k_{os} .

The algorithm is summarized in the pseudocode shown in Algorithm 1, and the corresponding block diagram is drawn in Fig. (3). Summarizing, after obtaining raw radar data, a 2D FFT is performed, followed by 2D-CA-CFAR [20]. With the obtained information, the initial ego-motion estimation is performed, and the motion-induced velocity is calculated and compared with the detected velocity. The detected points will be labelled, and the static targets will be sent to the iterative algorithm. These steps will be performed until the threshold is met and the final ego-motion estimation results obtained.

Algorithm 1 Proposed iterative method

Initialization.
 Obtain the velocity estimation for the detected targets $V_{dd}(m_k, n_k)$ and the initial estimation of translation speed $[v_x^1, v_y^1, v_z^1]$ with all the detected targets.
 Iteration i .
 Calculate the ego-motion induced velocity as in (8).
 Distinguish static targets based on the threshold as in (9).
 Form the new matrix for translation speed estimation \mathbf{T}_t^{i+1}
 Implement the pattern search algorithm for ego-motion estimation according to [12].
 $i = i + 1$
 Break the iteration when threshold is met.
 Obtain estimated results V_{ab} when using (10)
 Obtain estimated results V_{os} when using (12)
 Obtain estimated results V_{os-ab} when using (13)

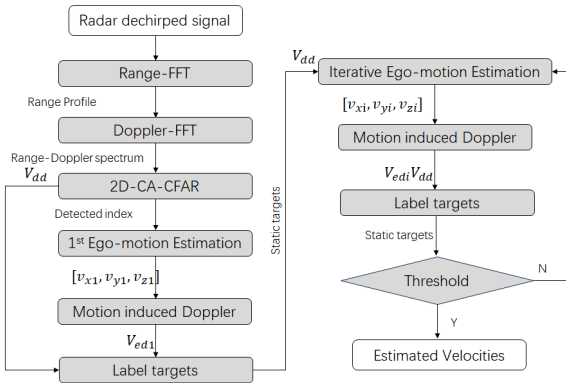


Fig. 3. Block diagram of the proposed method for ego-motion estimation.

IV. RESULTS AND DISCUSSION

To show the effectiveness of the proposed method, several results based on groups of simulated point targets are initially presented and analyzed. We used a simulated 8×8 2D uniform square array on the side-looking radar to evaluate the performance of the approach. The distances between different antennas are constant, $\frac{\lambda}{2}$, to avoid ambiguity. The radar parameters are listed in Table I. The ϵ in equation (10), (12) and (13) is set in the following simulations as 0.2.

Four hundred targets are generated in the radar field of view at random range values in the interval $[0 \text{ m}, 35 \text{ m}]$,

TABLE I
 RADAR PARAMETERS FOR THE VERIFICATION OF THE METHOD

Parameters	Value
Center Frequency (GHz)	77
Slope (MHz/us)	62.5
Sampling Rate (Msps)	32
Bandwidth (GHz)	1
PRI (us)	20
Number of chirps per frame	256

elevation in the interval $[-30^\circ, 30^\circ]$, and azimuth in the interval $[-60^\circ, 60^\circ]$. The amplitude of all scatterers is drawn from the uniform distribution $\alpha_o = \mathcal{U}(0, 300)$. According to the Swerling model III, the amplitude can be seen as constant during one coherent processing interval. The scatterers are also assumed to be isotropic and provide constant amplitude and phase of the scattered field during the processing period, as in [21]. The vehicle is moving with random speed selected from a uniform distribution in all three coordinates where $V_x = \mathcal{U}(-10.8 \text{ km/h}, 10.8 \text{ km/h})$, $V_y = \mathcal{U}(14.4 \text{ km/h}, 46.8 \text{ km/h})$, $V_z = \mathcal{U}(-10.8 \text{ km/h}, 10.8 \text{ km/h})$.

One example of the velocity plot cut at $\phi = 0$ is extracted from the velocity surface in Fig. 2. As shown in Fig. 4, the estimated ego-velocity results after three iterations of the proposed method are closer to the ground-truth than the estimation by the previous method [12].

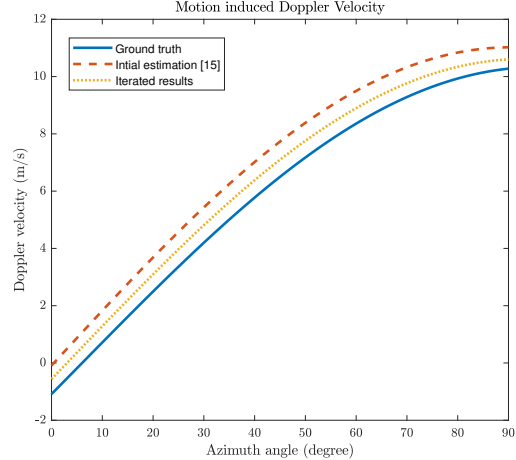


Fig. 4. Comparisons of estimated velocity with original [12] and proposed iterative method, compared to the ground truth when 40% targets are moving in $[0 \text{ m/s}, 6 \text{ m/s}]$.

To test performances under different ratios of moving targets, 100 Monte Carlo tests are performed. The moving targets' radial speeds are selected from a uniform distribution $v_r = \mathcal{U}(-21.6 \text{ km/h}, 21.6 \text{ km/h})$. The ratio of total moving targets ranges from 10% to 50%, as in common automotive scenarios many scatter points are often from static targets or clutter. The results for different threshold calculations ABT, OST, OS-ABT are compared in Figure 5. With the proposed

iterative method, the ego-motion estimation performances are improved compared with the conventional algorithm (blue line in the figure). The smaller the ratio of moving targets, the better improvement can be achieved. This is reasonable because outliers will show significant differences when the moving targets' ratio is lower, thus the iterative method can easily discard those outliers. However, as the moving targets' ratio increases, the differences become negligible because of high bias, reducing performances. Notably, the OS-ABT approach, as a combination of both advantages from ABT and OST, achieves the best results in almost every ratio and every direction. Only when the ratio of moving targets is small, i.e. 10%, the ABT approach already achieves good performance. The OS might introduce more bias by setting a fixed order which decreases slightly the performance.

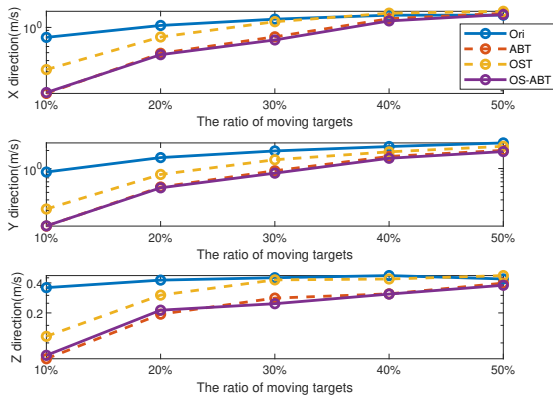


Fig. 5. Ego-motion estimation error in three directions, with different ratios of moving targets present in the scene and different termination thresholds approaches (ABT, OST, OS-ABT).

Another Monte Carlo test is performed, where 30% of targets in the field of view are simulated with random speeds. The radial speeds are chosen randomly in the range $[0 : v_r]$, with $v_r \in [3 \text{ m/s}, 6 \text{ m/s}, 9 \text{ m/s}]$. The results are shown in Fig. 6. As expected, the performance drops in all cases with increasing speeds because of the larger error introduced in the ego-motion estimation. Still, all the iterative algorithms reduce the estimated error of the ego-motion estimation. OS-ABT achieves the best results in all the directions and at all different speed ranges against the other two variants.

After testing different scenarios, i.e. different speeds of the targets and different ratios of moving targets, the parameters in the iterative algorithm are tested as well. D_c in equation (9) is tested with different values, namely $[0.5, 1, 1.5, 2, 2.5]$. D_c is used to determine the boundary between the static targets and the moving targets. If the value is too small, the constraint will be too strict, and the algorithm will highly rely on the initial estimation and stop easily at an inaccurate separation of targets. On the other hand, if the value is too large, more moving targets will be used for the final estimation, leading to a drop in the estimation accuracy. The results are shown in Fig. 7. The red boxes are from the original method [12],

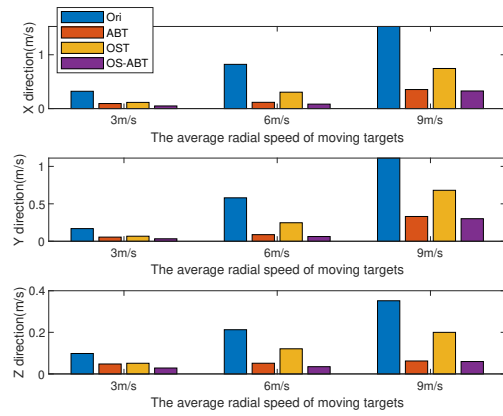


Fig. 6. Ego-motion estimation in three directions, with targets in the scene moving at different average speeds; different termination thresholds approaches compared (ABT, OST, OS-ABT).

which do not depend on D_c . We can see that ABT and OS-ABT obtain better results than OST. The outliers for OS-ABT are less than ABT, providing a lower variance estimation. The performances first improve from $D_c = 0.5$ to $D_c = 1.5$ by relaxing the strict constraint, but then the errors increases again with higher D_c values.

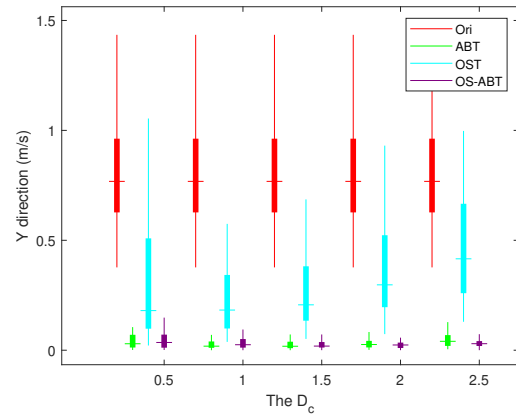


Fig. 7. Ego-motion estimation in three directions with different values of the parameter D_c for different termination thresholds approaches (ABT, OST, OS-ABT).

The ϵ and k parameters in the OST & OS-ABT are also tested with different values, and with moving targets' ratio equals to 30% and targets' speed range equals to 3m/s. The results show that for $k \geq 3$ the performance of the algorithm remains broadly constant, since the outliers are discarded in the iterations and only the static targets are selected.

Several extended targets in random shapes as shown in Fig. 8 are also simulated. All the targets within the maximum range of 100m for this simulation will be considered in the signal generation. Based on the signal model described in equation (1), the corresponding radar signals are generated from the superposition of the scatter points in each frame.

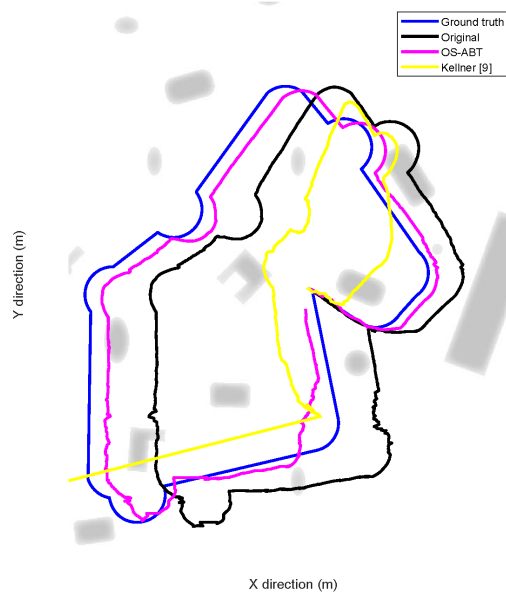


Fig. 8. Estimated trajectory using simulated data with different methods.

The ground truth trajectory and estimated trajectories are compared in Fig. 8 to evaluate the algorithm performance in a continuous, more realistic sequence of frames. With the proposed iterative approach, the estimated trajectory is moving closer to the ground truth. Three different evaluation metrics [12], namely absolute pose error (APE), absolute trajectory error (ATE) and relative trajectory error (RTE), are used to compare different ego-motion estimation algorithms. APE for the original algorithm is 1.4046 m/s, with the proposed algorithm 1.1154 m/s and the alternative method in [9] 54.29 m/s. ATE for the original algorithm is 79.1799 m, with the proposed algorithm 29.0577 m and the method in [9] 778 m. RTE calculated with 10 frames for the original algorithm is 2.4695 m, with the proposed algorithm 2.3209 m and the method in [9] 20.1m. All these evaluations prove that the proposed method improves the performance of the original algorithm [12].

V. CONCLUSION

This paper proposes an iterative method to improve the accuracy of the ego-motion estimation in scenarios with moving targets. The method compares the detected target velocity with the ego-motion-induced velocity, and targets with higher differences are labelled as moving targets, and then discarded in the next iteration. Thus, only static targets are selected for the final ego-motion estimation. Three different approaches to compute thresholds for the breaking point of the iterative method are proposed and compared as well.

The proposed method's effectiveness is verified through numerical simulations. The improvements are obtained under different moving ratios and different moving speeds (e.g., 3 times in 10% moving targets situations). Different threshold-based methods are compared with Monte Carlo tests, showing that the OS-ABT approach works robustly and accurately.

REFERENCES

- [1] F. Engels, P. Heidenreich, A. M. Zoubir, F. K. Jondral, and M. Wintermantel, "Advances in automotive radar: A framework on computationally efficient high-resolution frequency estimation," *IEEE Signal Processing Magazine*, vol. 34, no. 2, pp. 36–46, 2017.
- [2] Y. Almalioglu, M. Turan, C. X. Lu, N. Trigoni, and A. Markham, "Millirio: Ego-motion estimation with low-cost millimetre-wave radar," *IEEE Sensors Journal*, vol. 21, no. 3, pp. 3314–3323, 2020.
- [3] Y. Li, Y. Liu, Y. Wang, Y. Lin, and W. Shen, "The millimeter-wave radar slam assisted by the rcs feature of the target and imu," *Sensors*, vol. 20, no. 18, p. 5421, 2020.
- [4] A. Kramer, C. Stahoviak, A. Santamaria-Navarro, A.-A. Agha-Mohammadi, and C. Heckman, "Radar-inertial ego-velocity estimation for visually degraded environments," in *2020 IEEE International Conference on Robotics and Automation (ICRA)*. IEEE, 2020, pp. 5739–5746.
- [5] P. Wallrath and R. Herschel, "Egomotion estimation for a sensor platform by fusion of radar and imu data," in *2020 17th European Radar Conference (EuRAD)*. IEEE, 2021, pp. 314–317.
- [6] C. Doer and G. F. Trommer, "Radar visual inertial odometry and radar thermal inertial odometry: Robust navigation even in challenging visual conditions," in *2021 IEEE/RSJ International Conference on Intelligent Robots and Systems (IROS)*. IEEE, 2021, pp. 331–338.
- [7] O. Bialer and I. Bilik, "Accurate self localization using automotive radar synthetic aperture radar," Oct. 15 2019, uS Patent 10,444,347.
- [8] D. Kellner, M. Barjenbruch, J. Klappstein, J. Dickmann, and K. Dietmayer, "Instantaneous ego-motion estimation using doppler radar," in *16th International IEEE Conference on Intelligent Transportation Systems (ITSC 2013)*. IEEE, 2013, pp. 869–874.
- [9] —, "Instantaneous ego-motion estimation using multiple doppler radars," in *2014 IEEE International Conference on Robotics and Automation (ICRA)*, 2014, pp. 1592–1597.
- [10] M. Barjenbruch, D. Kellner, J. Klappstein, J. Dickmann, and K. Dietmayer, "Joint spatial-and doppler-based ego-motion estimation for automotive radars," in *2015 IEEE Intelligent Vehicles Symposium (IV)*. IEEE, 2015, pp. 839–844.
- [11] M. Rapp, M. Barjenbruch, M. Hahn, J. Dickmann, and K. Dietmayer, "Probabilistic ego-motion estimation using multiple automotive radar sensors," *Robotics and Autonomous Systems*, vol. 89, pp. 136–146, 2017.
- [12] S. Yuan, S. Zhu, F. Fioranelli, and A. Yarovoy, "3-d ego-motion estimation using multi-channel fmcw radar," *IEEE Transactions on Radar Systems*, 2023.
- [13] Y. S. Park, Y.-S. Shin, J. Kim, and A. Kim, "3d ego-motion estimation using low-cost mmwave radars via radar velocity factor for pose-graph slam," *IEEE Robotics and Automation Letters*, vol. 6, no. 4, pp. 7691–7698, 2021.
- [14] K. Haggag, S. Lange, T. Pfeifer, and P. Protzel, "A credible and robust approach to ego-motion estimation using an automotive radar," *IEEE Robotics and Automation Letters*, vol. 7, no. 3, pp. 6020–6027, 2022.
- [15] S. Lim, J. Jung, S.-C. Kim, and S. Lee, "Radar-based ego-motion estimation of autonomous robot for simultaneous localization and mapping," *IEEE Sensors Journal*, vol. 21, no. 19, pp. 21 791–21 797, 2021.
- [16] S. Yuan, F. Fioranelli, and A. Yarovoy, "Vehicular motion-based doa estimation with a limited amount of snapshots for automotive mimo radar," *IEEE Transactions on Aerospace and Electronic Systems*, 2023.
- [17] S. Yuan, P. Aubry, F. Fioranelli, and A. Yarovoy, "A novel approach to unambiguous doppler beam sharpening for forward-looking mimo radar," *IEEE Sensors Journal*, 2022.
- [18] S. Yuan, F. Fioranelli, and A. Yarovoy, "3drudat: 3d robust unambiguous doppler beam sharpening using adaptive threshold for forward-looking region," *IEEE Transactions on Radar Systems*, 2024.
- [19] C. Audet and J. E. Dennis Jr, "Analysis of generalized pattern searches," *SIAM Journal on optimization*, vol. 13, no. 3, pp. 889–903, 2002.
- [20] M. Weiss, "Analysis of some modified cell-averaging cfar processors in multiple-target situations," *IEEE Transactions on Aerospace and Electronic Systems*, no. 1, pp. 102–114, 1982.
- [21] M. Andres, P. Feil, and W. Menzel, "3d-scattering center detection of automotive targets using 77 ghz uwb radar sensors," in *2012 6th European Conference on Antennas and Propagation (EUCAP)*. IEEE, 2012, pp. 3690–3693.